Journal of the Korean Physical Society, Vol. 61, No. 3, August 2012, pp. 376∼386

Emission Spectroscopy Combined with a Single and a Double Probe in Low-pressure Inductively-coupled Nitrogen-Argon Plasmas

Jae Min Park, Min A Song and T. H. Chung*
Department of Physics, Dong-A University, Busan 604-714, Korea

(Received 3 January 2012, in final form 7 June 2012)

Low-pressure inductively coupled N_2-Ar plasmas have been studied to investigate the effects of operating parameters, including the Ar content, applied power, and gas pressure. By means of optical emission spectroscopy and single and double Langmuir probe diagnostic techniques, the evolutions of the plasma density, the electron temperature, and the N_2^+, N_2, N, and Ar emission lines have been investigated with a discussion of a spatially- averaged global model. From the emission spectra, the ratios of the concentrations of species of interest, and the rotational and the vibrational temperatures of the nitrogen molecules are obtained for various discharge conditions. The rotational and the vibrational temperatures of N_2 are found to increase with increasing applied power, pressure, and Ar content, thus making nitrogen plasmas more reactive.

PACS numbers: 52.25.Rv, 52.70.Kz, 52.20.Hv
Keywords: Inductively coupled nitrogen-Ar plasma, Optical emission, Langmuir probe
DOI: 10.3938/jkps.61.376

I. INTRODUCTION

Due to wide applications of plasma processes involving nitrogen, much effort has been devoted to the study of nitrogen plasmas [1–10]. Because the atomic nitrogen plays a key role in the synthesis of nitrides, the concentration of atomic nitrogen in nitrogen plasmas is a significant concern [1]. The common processing reactors utilizing inductively coupled plasmas (ICPs) and parallel-plate capacitive discharges have quite a low dissociation fraction. However, a recent global model predicts quite a high dissociation fraction of nitrogen molecules in ICP discharges [9]. One of the promising ways to enhance the dissociation of molecular nitrogen is to introduce another gas such as hydrogen and argon into nitrogen [1,4,11].

Major concerns in N_2-Ar plasmas include the measurement of plasma parameters and an understanding of the evolution of neutral particle densities with change in the operating parameters [12–14]. Neutral gas temperature is another important parameter because the neutral particle density changes with the neutral gas temperature for constant-pressure processes. The vibrational temperature represents the chemical reactivity of vibrational excited species [15]. In our previous works [16,17], we showed that increasing the Ar content caused significant changes in the properties of discharge such as the gas temperature, the rotational and the vibrational excitations, the electron energy distribution function, and the dissociation fraction of N_2 molecules. A higher Ar content caused an enhancement of the dissociation fraction. The calculated density of nitrogen atoms was found to be maximal at an Ar content of 30% for a fixed total gas pressure [16].

Understanding N_2-Ar plasmas constitutes a complex task due to the strong nonlinear coupling between the bulk kinetics of the numerous species in the discharge (electrons, ions, electronically and vibrational excited molecules, and atoms), the complexity of power transfer, and the effects of the plasma-wall interactions. In view of all plasma processes involving nitrogen-argon, it is therefore of importance to develop a detailed model combined with accurate and reliable diagnostic techniques to monitor the properties of N_2-Ar discharges [4,18]. However, it is also desirable to explain and predict the evolution of plasma parameters and neutral particle densities with change in the operating parameters based on a simple model rather than employing a complicated plasma chemistry model consisting of a huge number of reactions. It is worth providing a physical explanation of the behavior of the species concentration without relying on a full collisional-radiative model taking into account the creation and the loss mechanisms of plasma species.

In this work, a simple model for a low-pressure inductively coupled N_2-Ar discharge is established and utilized to investigate the effects of different operating parameters on the properties of the plasma. By means of optical emission spectroscopy and Langmuir (single and double) probe diagnostic techniques, the plasma parameters, such as the plasma density, electron temperature, and

*E-mail: thchung@dau.ac.kr

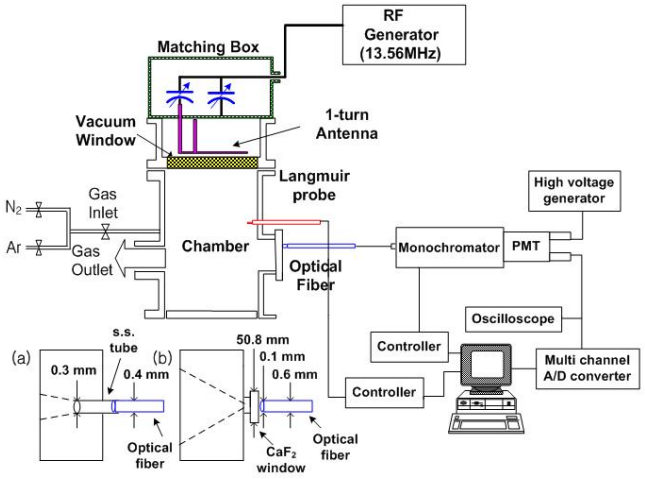

Fig. 1. (Color online) Schematic of the experimental setup.

concentrations of species of interest, are obtained. Especially, the electron temperature is a decisive parameter governing plasma chemical reactions; therefore, an accurate measurement of that is of importance. In addition, the rotational and vibrational temperatures of nitrogen molecules are obtained for various operating conditions. The variations in the species concentrations with pressure, power, and Ar content are investigated. A strong relationship among the plasma parameters, the species concentrations, and the rotational and vibrational temperatures is explored.

II. EXPERIMENT

1. Experimental Setup

A schematic diagram of the experimental setup with the diagnostics system (optical emission spectroscopy (OES), and Langmuir probe) is shown in Fig. 1. The plasma chamber consists of a stainless-steel cylinder with a 28-cm diameter and a 34-cm length. A 1.9-cm-thick by 27-cm-diameter tempered glass plate mounted on one end separates the planar one-turn induction coil from the plasma. The induction coil is made of copper (with water-cooling) and is connected to an L-type capacitive matching network and an rf power generator. The plasma chamber is evacuated by using a diffusion pump backed by a rotary pump, giving a base pressure of 5×10^{-6} Torr. The equilibrium gas pressure in the chamber is monitored with a combination vacuum gauge (IMG 300). The operating gas pressure is controlled by adjusting the mass flow controller. A 13.56-MHz generator (ENI OEM 12) drives an rf current in a flat one-turn coil through the matching network. To the nitrogen discharges generated, the argon was introduced as either an actinometer or as an adding gas. By changing the partial pressure of both gases, we varied the argon content in the range of 5 – 80% at a constant total pressure.

A diagnostics study of low-pressure planar inductively coupled plasmas (for applications in etching and deposition of thin films) using the nitrogen-argon mixture gas was performed by using OES and Langmuir probes. Both diagnostics complement one another to determine plasma parameters [19]. The experiments were conducted under the conditions of pressures in the range of 1 – 30 mTorr (with plasma on) and applied powers in the range of 160 – 600 W (most experiments performed in the H-mode of the ICP except the 160-W E-mode). To improve the reliability of the probe measurement, we obtained the electron density (n_e) and the electron temperature (T_e) by using both a single Langmuir probe (SLP 2000, Plasmart) and a double Langmuir probe (DLP 2000, Plasmart). The probe tip made of tungsten with a diameter of 0.5 mm and a length of 10 mm was located on the axis of the cylinder at 14 cm below the tempered glass plate. To measure the electron energy probability function (EEPF), we obtained the second derivatives of the probe current with respect to the probe potential, which is proportional to the EEPF, by numerically differentiating and smoothing.

2. Spectroscopic Evaluation Method

Light collection was made in two different positions. As shown in inset (a) of Fig. 1, an optical probe made of stainless-steel tube was inserted near the axis of the cylindrical chamber and was connected to an optical fiber outside the chamber. For inset (b), an optical fiber (0.1-mm slit diameter) attached to the CaF_2 window (5-mm thickness, 50.8-mm diameter) collected the light emission. The measured light intensities were volume-integrated with different solid angles (shown with dotted lines). The light intensities of emissive molecules and radicals in the plasma were focused by means of an optical fiber in entrance slit of a 0.75-m monochromator (SPEX 1702), equipped with a grating of 1200 grooves per millimeter and a slit width of 100 μm. The light was collimated at the exit slit where a photomultiplier tube (Hamamatsu R928) converted photons into an electric signal. The measured emission spectra should be corrected for the spectral response of the detection system, which includes the optical fiber, the monochromator, and the photomultiplier tube. The detection system had to be calibrated in intensity between 250 to 850 nm by using a quartz halogen lamp with a known spectral radiance. The dissociation fraction was obtained using the integrated intensity of the peaks of the emission spectra. For optical emission actinometry, spectral lines and bands from N_2 (337.1 nm, (C, 0) → (B, 0)), N_2^+ (391.4 nm, (B, 0) → (X, 0)), N (746.8 nm, 3p $^4S^0$ → 3s ^4P), Ar (750.4 nm, $2p_1 \rightarrow 1s_2$), and Ar (811.53 nm, $2p_9 \rightarrow 1s_5$) were chosen. The Ar* $2p_1$ level is very ef-

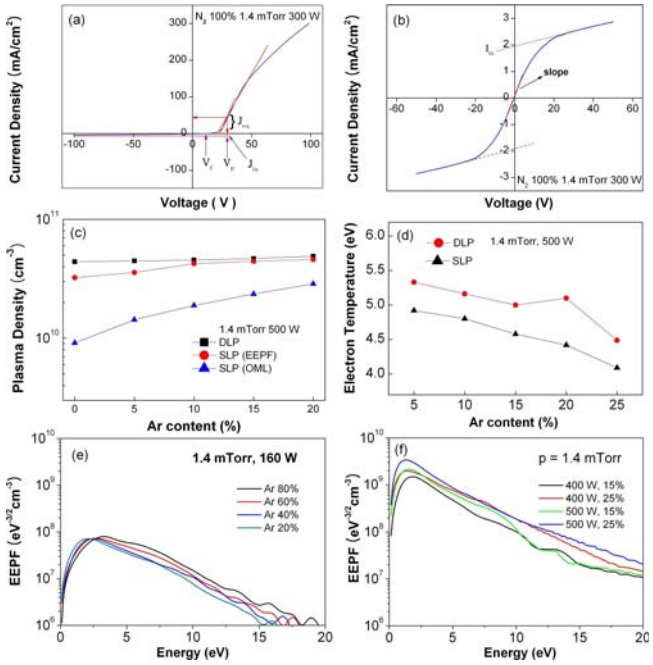

Fig. 2. (Color online) Probe current versus probe voltage of (a) the single probe and (b) the double probe. Here the determinations of the floating potential (V_f), plasma potential (V_p), ion saturation current density (J_{is}), and electron saturation current density (J_{es}) are shown. (c) Plasma density and (d) electron temperature obtained by using single Langmuir probe measurements as a function of the Ar content up to 20%. Electron energy probability functions (EEPFs) obtained by using the single probe for (e) E-mode (160 W) and (f) H-mode (400 W and 500 W) discharges. The gas pressure is fixed at 1.4 mTorr, and the Ar content is varied.

ficiently populated by electron-impact excitation from the ground-state whereas its population due to excitation from metastable states (Ar^m) is very inefficient [20]. There are two metastable Ar states, $1s_3$ ($^3P_0$) and $1s_5$ ($^3P_2$). The Ar^m ($^3P_2$) is effectively excited to the $2p_9$ state, in contrast to the $2p_2$ and the $2p_3$ levels which can be excited from both metastable levels [18,19]. Therefore, the $2p_9 \rightarrow 1s_5$ emission line (811.53 nm) provides useful information on the electron energy distribution in the plasma [21,22]. Because the reported populations of Ar^m ($^3P_2$) and Ar^m ($^3P_0$) are often close to the ratio of their statistical weights 5, the Ar^m($^3P_2$) density is representative of the total Ar^m density in the plasma [4,20]. The emission lines N (746.8 nm) and Ar (750.4 nm) overlap with the 740 – 755 nm range of the N_2 first positive system. However, the intensities of these lines can be measured by subtracting the levels of neighboring values (see the inset of Fig. 4(a)).

The assumption that a discharge is in a corona balance has allowed us to use a modified Boltzmann plot method to determine the electron temperature [23,24]. The gas temperature (T_g) is an important parameter because it must be known to determine neutral densities and ion-neutral mean free paths. The gas temperature of the N_2-Ar discharge can be deduced by measuring the rotational distribution of the first negative system of N_2^+, which is expected to be in equilibrium with T_g [25]. Equilibrium between translational and rotational modes can be strongly influenced by the formation mechanism of the emitting species [26]. Because high rotational energy is not imparted to N_2^+ during formation, many collisions with N_2 are necessary to achieve thermalization. The collision frequency between nitrogen molecules is high. Therefore, the rotational temperature of N_2^+ is assumed to be in equilibrium with the translational temperatures of N_2 and Ar. The rotational temperature of a molecule ($T_{\rm rot}$) can be obtained by comparing the synthetic diatomic molecular spectrum with the measured one [26,27]. The vibrational temperature ($T_{\rm vib}$) of nitrogen molecules can be obtained from the transition of the second positive system (N_2 (C, v') $\rightarrow$ N_2 (B, v'')) by using the Boltzmann plot method. Generally, the line intensity of the radiative transition of molecule can be expressed as [28]

$$\mathrm{I}_{(\mathrm{n}',\mathrm{v}',\mathrm{J}'\rightarrow\mathrm{n}'',\mathrm{v}'',\mathrm{J}'')} \propto \mathrm{h}\nu \mathrm{A}_{(\mathrm{n}',\mathrm{v}',\mathrm{J}'\rightarrow\mathrm{n}'',\mathrm{v}'',\mathrm{J}'')} \mathrm{N}_{\mathrm{n}',\mathrm{v}',\mathrm{J}'}, \quad (1)$$

where $\mathrm{I}_{(\mathrm{n}',\mathrm{v}',\mathrm{J}'\rightarrow\mathrm{n}'',\mathrm{v}'',\mathrm{J}'')}$ is the intensity of the spectrum (n is the electronic state, v is the vibrational quantum number, and J is the rotational quantum number), h is Planck's constant, ν is the frequency of the radiative transition, $\mathrm{A}_{(\mathrm{n}',\mathrm{v}',\mathrm{J}'\rightarrow\mathrm{n}'',\mathrm{v}'',\mathrm{J}'')}$ is the transition probability, and $\mathrm{N}_{\mathrm{n}',\mathrm{v}',\mathrm{J}'}$ is the number density of the molecules in the upper states.

When we assume a Boltzmann distribution for the vibrational and the rotational states, $\mathrm{N}_{\mathrm{n}',\mathrm{v}',\mathrm{J}'}$ can be rewritten as

$$\begin{aligned} \mathrm{N}_{\mathrm{n}',\mathrm{v}',\mathrm{J}'} &\rightarrow N_{n'} \exp\left(-\frac{E_{vib}}{kT_{vib}}\right)(2J'+1) \\ &\times \exp\left(-\frac{E_{rot}}{kT_{rot}}\right), \end{aligned} \quad (2)$$

where $N_{n'}$ is a constant independent of v and J, and E_{vib} and E_{rot} are the vibrational and the rotational energy levels, respectively. In this work, the values of T_e, T_{rot}, and T_{vib} are obtained as functions of different processing parameters of interest, such as the pressure, the applied power, and the Ar content.

3. Actinometric Technique

If two spectral line, 750.4 and 746.8 nm, are chosen for the OES actinometry [11], the dissociation fraction can be determined by calculating the ratio

$$\frac{[\mathrm{N}(2\mathrm{p}^4\mathrm{S}^0)]}{[\mathrm{N}_2]} = \frac{\mathrm{R}_{750}}{\mathrm{R}_{746}} \frac{\mathrm{v}_{750}}{\mathrm{v}_{746}} \frac{\mathrm{A}_{750}}{\mathrm{A}_{746}} \frac{\mathrm{k}_{\mathrm{Ar}}^{\mathrm{dir}}}{\mathrm{k}_{\mathrm{N}}^{\mathrm{dir}}} \frac{\tau_{\mathrm{Ar}}}{\tau_{\mathrm{N}}} \frac{[\mathrm{Ar}]}{[\mathrm{N}_2(\mathrm{X})]} \frac{\mathrm{I}_{746}}{\mathrm{I}_{750}}. \quad (3)$$

Here, R is the spectral response of the system, A is the emission probability, v is the frequency, τ is the life-time

(which is the inverse of the sum of the emission probabilities for all the radiative de-excitation processes) at the chosen spectral lines, k_{Ar}^{dir} is the rate coefficient for electron-impact direct excitation to Ar* ($2p_1$) from the ground-state Ar, k_N^{dir} is the rate coefficient for electron-impact direct excitation to N* ($3p\ ^4S^0$) from the ground-state N, and I is the emission line intensity. Quenching is negligible in the low-pressure plasmas considered in this work. [Ar]/[N_2(X)] is the gas mixing ratio. The low accuracy for the excitation cross-section data involved in the calculation of the rate coefficient ratio k_N^{dir}/k_{Ar}^{dir} may make a quantitative determination of the dissociation fraction difficult [4].

For discharges with higher Ar contents, the density of Ar^m may become important and, as a consequence, the Ar* ($2p_1$) state may be created from the Ar^m by electronic collisions, so the actinometry may no longer be valid [29]. The production of N* ($3p\ ^4S^0$) has several routes other than the direct excitation of the ground state N. They include electronic excitation of the metastable state N^m, electronic excitation through dissociation of the molecule N_2, and excitation of N* to N* ($3p\ ^4S^0$) due to collisions with Ar* (mainly Ar^m) and with excited N_2*. However, the Ar^m is efficiently quenched by N_2 and N, and the production of these states in low-pressure discharges is not significant. Moreover, the population of N^m is 6 – 10 times lower than that of the ground-state N and the rate coefficient for the electronic excitation of the metastable state N^m to N* ($3p\ ^4S^0$) is less than k_N^{dir} by a factor of 10 at $T_e = 5$ eV [4]. The dissociative excitation rate coefficient is less than k_N^{dir} by a factor of 10^3 at $T_e = 4 - 5$ eV [4].

The measured emission intensity from the Ar* atom ($2p_1 \rightarrow 1s_2$), I^*_{750}, is written as

$$\begin{aligned} I^*_{750} &= I_{750}(1 + c_2), \\ I_{750} &= R_{750} h\nu_{750} A_{750} \tau_{750} n_e [Ar] k_{Ar}^{dir}, \\ c_2 &= \frac{[Ar^m(^3P_0)] k_{exc}^{Ar^{m0}}}{[Ar] k_{Ar}^{dir}}, \end{aligned} \tag{4}$$

where c_2 is the correction factor accounting for the excitation from the Ar^m, $k_{exc}^{Ar^{m0}}$ is the rate coefficient for the reaction e + Ar^m ($^3P_0$) → e + Ar* ($2p_1$). Note that c_2 depends mainly on T_e. Similarly, the measured emission intensity from the Ar* atom ($2p_9 \rightarrow 1s_5$), I^*_{811}, is written as

$$\begin{aligned} I^*_{811} &= I_{811}(1 + c_3), \\ I_{811} &= R_{811} h\nu_{811} A_{811} \tau_{811} n_e [Ar] k_{Ar}^{dir-2p_9}, \\ c_3 &= \frac{[Ar^m(^3P_2)] k_{exc}^{Ar^{m2}}}{[Ar] k_{Ar}^{dir-2p_9}}, \end{aligned} \tag{5}$$

where $k_{Ar}^{dir-2p_9}$ is the rate coefficient for electron-impact direct excitation to Ar* ($2p_9$) from the ground-state Ar, and c_3 is the correction factor accounting for the excitation from the Ar^m ($k_{exc}^{Ar^{m2}}$ is the rate coefficient for the reaction e + Ar^m ($^3P_2$) → e + Ar* ($2p_9$)). The atom-collision population transfer in the 2p level is neglected because the atom-collision rate is very small compared to the rate of electron-impact excitation in low-pressure plasmas. Also, the stepwise excitations that usually occur from 1s metastables are neglected.

From Eqs. (4) and (5), we have

$$\frac{I^*_{811}}{I^*_{750}} = \frac{R_{811}}{R_{750}} \frac{\nu_{811}}{\nu_{750}} \frac{A_{811}}{A_{750}} \frac{k_{Ar}^{dir-2p_9}}{k_{Ar}^{dir}} \frac{\tau_{811}}{\tau_{750}} \frac{1 + c_3}{1 + c_2}. \tag{6}$$

As will be shown in Fig. 4, the ratio $k_{Ar}^{dir-2p_9}/k_{Ar}^{dir}$ is found to be close to 1. The factors c_2 and c_3 contain the densities of Ar^m, and all the rate coefficients therein can be represented as a function of T_e. If T_e is determined, the measured ratio of I^*_{811}/I^*_{750} can be used to estimate the Ar^m density by using Eqs. (4) – (6).

Table 1. Spectral responses and spectroscopy data for the selected transitions.

R	λ (nm)	Transition	τ (ns)	A ($\times 10^7$ s^{-1})
0.0185	746.8	N ($3p\ ^4S^0 \rightarrow 3s\ ^4P$)	26.3	1.9
0.0158	750.4	Ar ($2p_1 \rightarrow 1s_2$)	21.3	4.45
0.0068	811.5	Ar ($2p_9 \rightarrow 1s_5$)	30.2	3.31
0.479	337.1	N_2 (C, 0) → (B, 0)	37	1.41
0.448	391.4	N_2^+ (B, 0) → (X, 0)	60	1.2

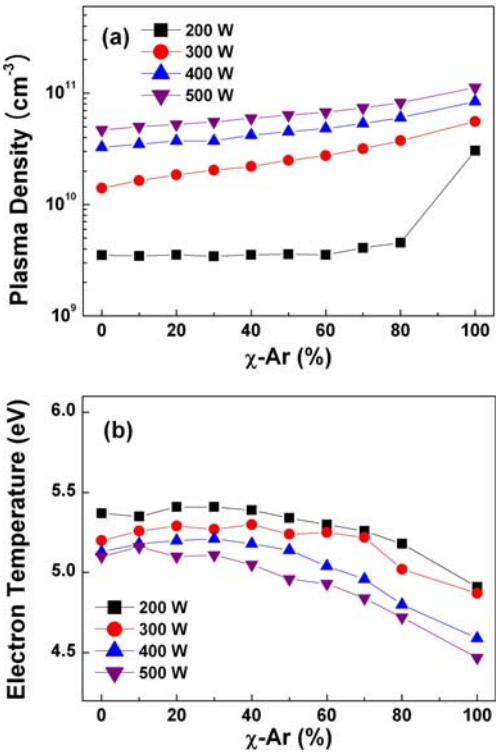

Fig. 3. (Color online) (a) Plasma density and (b) electron temperature obtained by using double probe measurements as a function of Ar content. The gas pressure is fixed at 1.4 mTorr, and the power is varied from 200 W to 500 W.

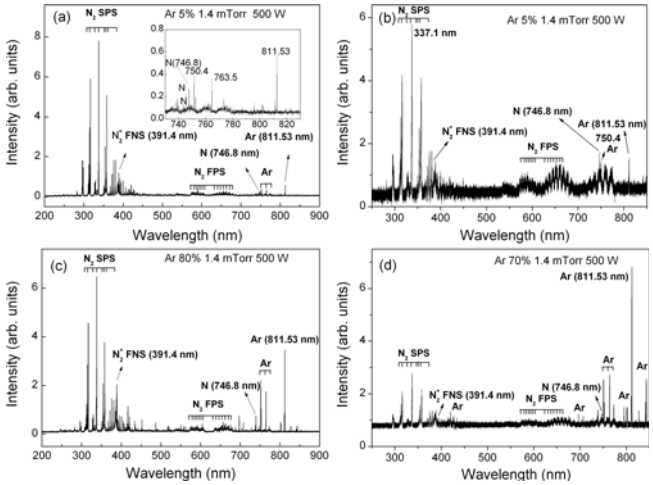

Fig. 4. Representative optical emission spectra from ICP N_2-Ar discharges at p = 1.4 mTorr and P = 500 W ((a) Ar-5% obtained at the CaF_2 window, (b) Ar-5% obtained by using an optical probe, (c) Ar-80% obtained at the CaF_2 window, and (d) Ar-70% obtained by using an optical probe). The inset in (a) presents the spectrum for the wavelengths of 730 – 830 nm.

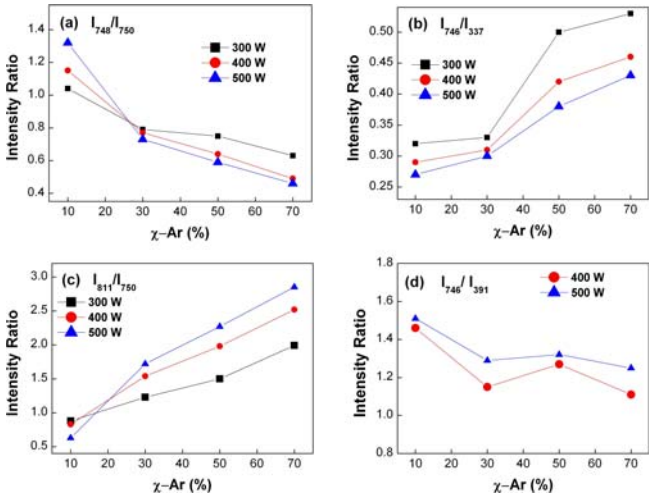

Fig. 5. (Color online) Intensity ratios of chosen spectral lines as functions of the Ar content in the mixture at p = 1.4 mTorr: (a) I_{746}/I_{750}, (b) I^*_{811}/ I^*_{750}, (c) I_{746}/I_{337}, and (d) I_{746}/I_{391}.

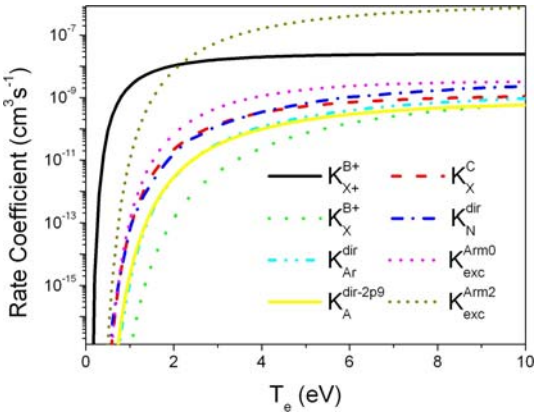

Fig. 6. (Color online) Rate coefficients as a function of T_e for the electron-impact excitation or ionization: from the ground state Ar ($1s_0$) to Ar ($2p_1$) (k_{Ar}^{dir}), from Ar($1s_0$) to Ar ($2p_9$) ($k_{Ar}^{dir-2p_9}$), from the metastable state Ar($1s_3$) to Ar ($2p_1$) ($k_{exc}^{Ar^{m0}}$), from the metastable state Ar($1s_5$) to Ar($2p_9$) ($k_{exc}^{Ar^{m2}}$), for direct excitation of ground state N to N^* ($3p\ ^4S^0$) state (k_N^{dir}), from ground state N_2 (X) to N_2 (C) (k_X^C), from ground state N_2^+(X) to N_2^+(B) ($k_{X^+}^{B^+}$), and for ionization from ground state N_2 (X) to N_2^+(B) ($k_X^{B^+}$).

Assuming that nitrogen molecules in the ground state N_2(X) constitute the dominant species, that the main reaction of excitation of state N_2(C) is electron impact excitation from the ground state N_2, and that levels of N_2(C) are primarily lost by radiative decay, the intensity of the emission line N_2 (337.1 nm, (C, 0) → (B, 0)) can be written as

$$I_{337} = R_{337} h\nu_{337} A_{337} \tau_{337} n_e [N_2] k_X^C, \quad (7)$$

where k_X^C is the rate coefficient for the reaction e + N_2 (X) → N_2 (C) + e, and the excitation reaction from the Ar^m (N_2(X) + Ar^m → N_2(C) + Ar) and the pooling reaction N_2(A) + N_2(A) → N_2(C) + N_2(X) can be neglected [30].

From Eqs. (3) and (7), we have

$$\frac{[N(2p\ ^4S^0)]}{[N_2]} = \frac{R_{337}}{R_{746}} \frac{\nu_{337}}{\nu_{746}} \frac{A_{337}}{A_{746}} \frac{k_X^C}{k_N^{dir}} \frac{\tau_{337}}{\tau_{746}} \frac{I_{746}}{I_{337}}. \quad (8)$$

The coefficient ratio k_X^C/k_N^{dir} is a decreasing function of T_e. The ratio is about 2 at $T_e = 3$ eV and 1.6 at $T_e = 5$ eV [4]. Likewise, N_2^+(B) can be considered to be mainly excited by electron-impact collision from the ground state of N_2^+ and levels of N_2^+(B) can be considered to be primarily lost by radiative decay [30]. Then, we have

$$\frac{[N(2p\ ^4S^0)]}{[N_2^+(X)]} = \frac{R_{391}}{R_{746}} \frac{\nu_{391}}{\nu_{746}} \frac{A_{391}}{A_{746}} \frac{k_{X^+}^{B^+}}{k_N^{dir}} \frac{\tau_{391}}{\tau_{746}} \frac{I_{746}}{I_{391}}, \quad (9)$$

where $k_{X^+}^{B^+}$ is the rate coefficient for the reaction e + N_2^+(X) → N_2^+(B) + e , and the correction accounting for the excitation reaction from the Ar^m (N_2^+(X) + Ar^m → N_2^+(B) + Ar) is neglected. The contribution from the reaction e + N_2(X) → N_2^+(B) + e (rate coefficient: $k_X^{B^+}$) can also be neglected because of the high threshold energy of 18.7 eV and smaller cross section [30]. The excitation to N_2^+(B) also takes place by collision of N_2^+(X) with vibrationally-excited molecules N_2(X, $v >$ 12) through the reaction N_2^+(X) + N_2(X, $v > 12$) → N_2^+(B) + N_2(X, v – 12). However, this reaction is not included in Eq. (9). If the evolutions of the emission intensities and rate coefficients (which will be shown in Fig. 5 and Fig. 6) are used, the concentration ratios of species can be obtained for various discharge conditions.

The spectral responses and spectroscopic data for the selected transitions used in Eqs. (3) – (9) are listed in Table 1.

III. RESULTS AND DISCUSSION

1. Probe Measurements of Plasma Parameters

The plasma density and the electron temperature of inductively coupled N_2-Ar plasmas were measured by using both a single probe and a double probe. For the single probe measurement, there are several methods of interpreting the probe I-V curve to obtain n_e and T_e. In this work, the plasma density was obtained either by using the integral of EEPF or by using orbital-motion-limited (OML) theory and it was considered as the electron density. Figures 2(a) and (b) represent the probe current-voltage curves for the single probe and double probe, respectively. The electron temperatures obtained by using the double probe are found to be a little larger than those measured by using the single Langmuir probe and by using OES. The double probe has the advantage that the net current never exceeds the ion saturation current, minimizing the disturbance to the discharge, but has a consequent disadvantage that only the high-energy tail of the electron distribution is collected by either probe. Therefore, as shown in Figs. 2(c) and (d), the double probe provides a little higher n_e and T_e than that obtained by using the single probe. The plasma densities obtained from the integrals of the EEPF were a little larger than those obtained from the OML theory. However, the tendency of variations of n_e and T_e with the Ar content remained unchanged. Even when the Ar was introduced into gas mixture in a small amount, many routes of excitation of Ar atom rather than electron-impact excitation from the ground state Ar existed. Collisions between nitrogen species and Ar atom (and between Ar^* and Ar atom) can cause the Ar excitations. This may also cause some deviation from the corona balance. This may be another reason for the difference between the probe results and the OES results. Figures 2(e) and (f) show the measured EEPFs at various Ar contents in the E-mode (ICP power of 160 W) and the H-mode (400 W and 500 W). The shape of the EEPF is observed to roughly remain Maxwellian. This was also observed in higher Ar-content N_2-Ar plasmas in the H-mode [16,17].

Next, the Ar content was varied in the range of 0 – 100% in the double Langmuir probe experiment for different powers at a pressure of 1.4 mTorr. As shown in Figs. 3(a) and (b), the plasma density was found to increase with increasing power and Ar content whereas the electron temperature decreased (even though T_e exhibited a different behavior depending on the power and in the region of a low Ar content up to 30%, but repeated measurements indicated this tendency as seen in Fig. 2(d)). This can be explained by using a spatially-averaged model of particle and power balance. The particle balance in N_2-Ar plasmas can be written as

$$k_{iz}^{N_2}[N_2] + k_{iz}^{N}[N] + k_{iz}^{Ar}[Ar] = \frac{u_B}{d_{eff}}, \quad (10)$$

where $k_{iz}^{N_2}$, k_{iz}^{N}, and k_{iz}^{Ar} denote the rate coefficients of the electron impact ionization of N_2, N, and Ar, respectively, u_B is the Bohm velocity, and d_{eff} is the effective length of the plasma chamber. Equation (10) governs the behavior of T_e. If the Arrhenius form is utilized [9], the rate coefficients $k_{iz}^{N_2}$, k_{iz}^{N}, and k_{iz}^{Ar} have similar dependences on T_e; therefore, the Ar content has little influence on T_e. The power balance equation relates the electron density to the absorbed power (P_{abs}) as

$$n_e = \frac{P_{abs}}{eA_{eff}\left(\varepsilon_c^{N_2}\delta_{N_2^+} + \varepsilon_c^{N}\delta_{N^+} + \varepsilon_c^{Ar}\delta_{Ar^+} + \varepsilon_e + \varepsilon_i\right)}, \quad (11)$$

where A_{eff} is the effective surface area of the chamber, and $\delta_{N_2^+} = [N_2^+]/n_e$, $\delta_{N^+} = [N^+]/n_e$, and $\delta_{Ar^+} = [Ar^+]/n_e$ are relative concentrations of charged species with respect to the electrons. Here, $\varepsilon_c^{N_2}$ and ε_c^{N} are the collisional energy losses per ionization event of nitrogen molecules and nitrogen atoms, respectively, and ε_c^{Ar} is the collisional electron energy loss per ionization event of argon gas. The average energy of escaping ions, ε_i, is the sum of the ion energy entering the sheath $T_e/2$ and the energy gained in the sheath V_{sh} (sheath voltage drop), and ε_e is the average energy of electrons escaping to the walls and is assumed to be equal to 2 T_e. As the Ar content increases, the term $\varepsilon_c^{N_2}\delta_{N_2^+} + \varepsilon_c^{N}\delta_{N^+} + \varepsilon_c^{Ar}\delta_{Ar^+}$ decreases because $\varepsilon_c^{N_2}\delta_{N_2^+}$ and $\varepsilon_c^{N}\delta_{N^+}$ are several times larger than $\varepsilon_c^{Ar}\delta_{Ar^+}$ at $T_e = 3$ – 5 eV. For a fixed power, with increasing Ar content, the collisional energy loss per electron-ion pair decreases; hence, the plasma density increases due to the power balance. In the case of a high-Ar-content plasma, the collisional energy loss decreases with increasing absorbed power due to the increase in the multistep ionizations; thus, the plasma density increases [31].

With varying Ar content, the plasma density had values ranging from 3.5×10^9 to $1.1 \times 10^{11}/cm^3$, and the electron temperature had values ranging from 4.4 to 5.4 eV. At low pressure ($p = 1.4$ mTorr), T_e decreases slightly with increasing Ar content, but remains above 4 eV. In this case, N_2^+ is mainly ionized by electron-impact ionization of N_2, and the discharge maintains excessive Ar^*. This explains the behaviors of the variations of I_{746}/I_{337} and I_{746}/I_{391} in Fig. 5. Because the ionization potential of Ar (15.76 eV) is comparable to those of N (14.5 eV) and N_2 (15.58 eV), T_e is not expected to change much with the Ar content. As the power increases, T_e is observed to decrease. This can be attributed to the effect of molecular dissociation, which increases with power. With T_e almost unchanged, an increase in the plasma density with increasing Ar content

results in the production (and excitation) of N atoms. However, the increase rate of I_{391} is a little larger than that of I_{746}, as shown in Fig. 5. Accurate values of n_e and T_e are also necessary to estimate the correction factor in evaluating the dissociation fraction at an arbitrary Ar content, which was described in our previous work [17].

2. Evolution of Spectral Bands and Lines with Control Parameters

The N_2-Ar plasma contains N_2 molecules, N_2^+ and Ar^+ ions, N and Ar atoms and their excited states, and electrons. Four representative optical emission spectra from the nitrogen-argon plasma are shown in Fig. 4. Figures 4(a) and 4(c) are the spectra obtained through the CaF_2 window at Ar-5% and Ar-80%, respectively. The spectra obtained by using the inserted optical probe, shown in Figs. 4(b) and 4(d) (Ar-70%), exhibited weaker intensities and higher noise level because the light travels in a 20 cm-long stainless steel tube before coming into the optical fiber. Besides the Ar peaks, most of the peaks and bands originate from the second positive system (SPS: N_2 (C) $\rightarrow$ N_2 (B)). The varieties of lines and band structures originate in the numerous rotational and vibrational levels between which transitions can occur. Two other features are present. They are a transition at 391.4 nm (the first negative system (FNS), N_2^+(B) $\rightarrow$ N_2^+(X)) and the appearance of the first positive system (FPS: N_2 (B) $\rightarrow$ N_2 (A)). For a discharge with a higher Ar content, the intensity of Ar peaks increases up to a level comparable to (or higher than) those of the nitrogen molecular bands, depending on the gas pressure. In the spectra obtained through the CaF_2 window, the intensities of N_2 peaks become stronger, and the intensities of Ar and N peaks are relatively weak. As the Ar contents increased, however, the intensities of Ar peaks increase more remarkably in the spectra obtained by using the inserted optical probe than in the spectra obtained through the CaF_2 window. This might be related to the detection solid angle and to the length of the integration line. The light collection through the CaF_2 window provides a larger solid angle and longer integration line, thus increasing the intensity far beyond the noise level. The effects of the Ar content and the applied power on the emission intensity of the spectral lines were investigated.

The Ar content was varied in the range of 5 – 80%. In the spectra obtained by using the optical probe, the N_2 337.1-nm peak was higher than the Ar peak at 811 nm for the case of a 5% - Ar discharge (Fig. 4(b)). The dominant peaks due to the Ar transition were higher than the second positive system peak (337.1 nm) in the discharges above an Ar content of 30%. Above an Ar content of 20%, the light emission intensities from Ar (750.4 and 811.5 nm) begin to exceed those from N and N_2^+. However, the intensity of light emission from the nitrogen second positive system remains almost unchanged as the Ar content is increased. The continuous increases in the intensities from Ar lines (811.5, 763.6, 801.4, 696.5 nm) indicate strong transitions to the Ar^m ($^3P_2$) (Fig. 4(d)). On the other hand, in the spectra obtained through the CaF_2 window, the intensities of the N_2 second positive system were much higher than those of Ar peaks (Fig. 4(a)). This tendency continues in the case of higher Ar content (Fig. 4(c)). Since the intensities of N (746.8 nm), Ar (750.4 nm), and Ar (811.53 nm) are mainly utilized for actinometry, either position of the light collection gave similar intensity ratios between the lines (especially 746.8 and 750.4 nm). If not mentioned otherwise, the analysis was performed based on the spectrum obtained through the CaF_2 window.

In low-pressure nitrogen plasmas, there are two main generation channels of the N_2 (C) state. The first one is by electron impact on the ground state of the nitrogen molecule N_2 (X). Another excitation channel is the collision of the ground-state nitrogen molecule or the metastable nitrogen molecule (N_2 (A)) with Ar^m [32]. Although the N_2 gas (N_2 (X)) supply is decreased with increasing Ar content, the light intensity from N_2 (337.1 nm (C, 0) $\rightarrow$ (B, 0)) remains unchanged due to the excitation channel caused by Ar^m. As the Ar content is increased, the intensities from N^* (3p $^4S^0$) and N_2^+ (B) increase slightly due to the enhanced excitation caused by collisions with generated Ar^m. This can be accounted for by charge transfer (Ar^+ + N_2 (X) $\rightarrow$ Ar + N_2^+ (X, v)), followed by electron impact excitation (e + N_2^+ (X) $\rightarrow$ e + N_2^+ (B)). The production of N_2^+ (B) is also caused by the collisional excitation of the ground state N_2^+ (X) with nitrogen molecules in highly-excited vibrational states N_2 (X, v > 12) [24]. The N_2^+ line at 391.4 nm is also enhanced slightly due to Penning ionization (Ar^* + N_2 (C) $\rightarrow$ Ar + N_2^+ (B) + e). An impact of Ar^m leads to the dissociation of N_2 and the recombination to N_2 in vibrationally-excited states (the recombination occurs near the chamber walls) [33].

Figure 5 shows the variations of the intensity ratios of the chosen spectral lines obtained by using the optical probe as a function of the Ar content. As shown in Fig. 5(a), the ratio I_{746}/I_{750} is observed to decrease with increasing Ar content, which indicates that the population of Ar^* ($2p_1$) is increased more than that of N^* (3p $^4S^0$) with increasing Ar content. The I_{N2} is not much affected by the Ar content. This can be explained as follows: Although the feed N_2 gas is decreased with increasing Ar content, the population of Ar^m is increased, and its collision with N_2(X) results in a larger population of N_2(C) (and also N_2^+ via e + N_2 (C) $\rightarrow$ N_2^+ + 2e). These cause the I_{N_2} to remain not much changed with changing Ar content. Although I_{N_2} is increased slightly or remains unchanged with increasing Ar content, I_N is more increased due to the charge transfer reaction (Ar^++ N_2 $\rightarrow$ N_2^+ + Ar), followed by the dissociative recombination e + N_2^+ $\rightarrow$ N + N. The relative content of Ar^* increases with continually increasing Ar content. This also contributes to the dissociation of N_2 via Ar^* + N_2

→ N + N + Ar [34]. Therefore, the ratio I_{746}/I_{337} turns out to increase with increasing Ar content (Fig. 5(b)). The ratio I_{746}/ I_{337} is observed to decrease slightly with increasing power. The reason for this may be that an increase in the production rate of N with increasing power is a little less than that in the excitation rate of N_2.

The ratio I_{811}/I_{750} is observed to increase with increasing Ar content (Fig. 5(c)). This can be explained by the population of Ar^m increasing with increasing Ar content more rapidly than that of Ar^* ($2p_1$) [32,33]. This is also related to a decrease in the electron temperature with increasing Ar content. The line intensity ratio $I^*{}_{811}/I^*{}_{750}$ is an indicator of changes in the electron energy distribution function and depends on the electron temperature. As the power increases, the ratio exhibits a slight increase. This is because the power increases, T_e decreases slightly, and although both the populations of the Ar^m and the resonant state Ar^* ($2p_1$) are increased, the Ar^m population is increased more rapidly [4]. As the discharge is shifted to the Ar-dominating region, the intensity levels of the Ar transition become large and the rate of increase of the intensity with increasing power becomes large.

As shown in Fig. 5(d), the ratio I_{746}/I_{337} increases with increasing Ar content; then, according to Eq. (8), the ratio [N (2p $^4S^0$)]/[N_2] increases with increasing Ar content (because the ratio of the rate coefficients does not vary much with the Ar content), which supports the actinometry result from the ratio $I_{746}/I^*{}_{750}$. However, considering the contributions from Ar^m to the increases in both [N (2p $^4S^0$)] and [N_2] , the rate of increase of [N (2p $^4S^0$)]/[N_2] with increasing Ar content would be smaller than that of I_{746}/I_{337}. From Fig. 5(d) and Eq. (9), the ratio [N (2p $^4S^0$)]/[$N_2{}^+$(X)] is expected to increase a little with increasing power and to decrease with increasing Ar content. However, some attention should be paid in using Eqs. (8) and (9). The operating parameters (pressure, power, especially the Ar content) were observed to have a noticeable influence on the intensities of the emission lines from the N_2 second positive system and the $N_2{}^+$ first negative system, which indicates a change in the vibrational energy distribution of nitrogen molecules. Therefore, the intensities at 337.1 nm and 391.4 nm depend on the vibrational temperature. The rate coefficients k_X^C and $k_{X^+}^{B^+}$ are estimated without consideration of the vibrational states; thus, Eqs. (8) and (9) can only be used in an approximate manner.

Generally all intensities from N_2, $N_2{}^+$, N, and Ar are observed to increase with increasing applied power. Especially, the intensity levels of N and $N_2{}^+$ are relatively small, and their rates of increase with increasing power are small, but the rates of increase and the intensity levels depend on the Ar content. In a nitrogen-dominated region, I_{337} is the highest, the rest of the lines have comparable intensity levels, and the rates of increase with increasing power are moderate. In pure nitrogen plasmas, the electron-impact dissociation reaction (e + N_2 → e + N + N) is more effective for N atom production than dissociative recombination (e + $N_2{}^+$ → N + N). In a nitrogen-dominated discharge with some addition of Ar, the main mechanism of N production is also direct electron-impact dissociation of N_2. In a nitrogen-dominated region, the productions of N and $N_2{}^+$ are closely related because that N atoms are mainly produced by electron-impact dissociation or dissociative recombination while $N_2{}^+$ is produced by electron-impact ionization (e + N_2 → $N_2{}^+$ + 2e) with a cross section at the same level as that of electron-impact dissociation [4]. On the other hand, some production routes of N and the destruction route $N_2{}^+$ are connected, and electron-ion recombination reactions (e + $N_2{}^+$ → N + N) are very efficient at low electron energy. In this region, $I_{N_2^+}$ is also observed to increase slightly with increasing Ar content because of the increase in the charge transfer collision mentioned above. However, I_N has a larger value than $I_{N_2^+}$ in this region. Therefore, the relative ratio of the intensities from N to $N_2{}^+$ is larger in a nitrogen-dominated region. On the other hand, in an Ar-dominated region, the production of $N_2{}^+$ is increased more due to the charge transfer reaction, and the rate of increase of the $N_2{}^+$ density is a little larger than that of N density. As the Ar content is increased, [Ar^m] also increases, and this promotes the Penning excitation (Ar^m + $N_2{}^+$(X) → $N_2{}^+$(B) + Ar). Then, the transition $N_2{}^+$(B) → $N_2{}^+$(X) (391.4 nm) becomes frequent, thus making I_{391} intense. Therefore, the ratio I_{746}/I_{391} decreases slightly with increasing Ar content.

By observing the OES spectra carefully, we can observe that ICP N_2-Ar plasmas are promising sources of active species such as ground-state N (^4S) atoms, $N_2{}^+$ ions, and metastable N_2 (A) molecules. From the N_2 first positive system, it is evident that the relative populations of N_2 (A) and N_2 (B) increase with increasing Ar content [11]. From the Ar peaks at 772.4 nm, 794.8 nm, and 811.5 nm, the relative number of Ar^m ($^3P_0$, $^3P_2$) can be observed to increase. The effective excitation transfer from the Ar^m ($^3P_0$, $^3P_2$) to the N_2 (C $^3\prod_u$) state also contributes to the N_2(A $^3\Sigma_u{}^+$) population through the fast radiative decay of the N_2 (C $^3\prod_u$) state to N_2 (B $^3\prod_g$). The rate coefficients are calculated using the cross section data as

$$K_j = \sqrt{\frac{2e}{m_e}} \int_0^\infty \sigma_j(E)\sqrt{E}\, f(E)dE, \qquad (12)$$

where e and m_e are the charge and the mass of the electrons, respectively, σ_j is the electron-impact cross section of collision type j, and f(E) is the electron energy distribution function. With the cross section data in the literature [30,35-37] and Maxwellian electrons, the rate coefficients for the direct excitation from the ground- state Ar($1s_0$) to Ar ($2p_1$) (k_{Ar}^{dir}), from the ground-state Ar($1s_0$) to Ar ($2p_9$) ($k_{Ar}^{dir-2p_9}$), from the metastable state Ar($1s_3$) to Ar ($2p_1$) ($k_{exc}^{Ar^{m0}}$), from the metastable state Ar($1s_5$) to Ar($2p_9$) ($k_{exc}^{Ar^{m2}}$), from the ground state N to N* (3p

$^4S^0$) state (k_N^{dir}), from the ground-state N_2 (X) to N_2 (C) (k_X^C), and from the ground-state N_2^+(X) to N_2^+(B) ($k_{X^+}^{B^+}$), as well as for the ionization from the ground-state N_2 (X) to N_2^+(B) ($k_X^{B^+}$), are computed and presented as functions of T_e in Fig. 6. At a typical $T_e = 3$ eV, we have an ordering such as $k_{exc}^{Ar^{m2}} > k_{X^+}^{B^+} > k_{exc}^{Ar^{m0}} > k_X^C \cong k_N^{dir} > k_{Ar}^{dir} \cong k_{Ar}^{dir-2p_1} > k_X^{B^+}$. Although the excitation routes to Ar ($2p_1$), Ar($2p_9$), N* (3p $^4S^0$), N_2 (C) and N_2^+(B) are over-simplified, the OES model consisting of Eqs. (3) – (9) (with T_e determined) can provide a useful tool to explain and predict the evolutions of the densities of plasma species with changing operating parameters.

3. Plasma Temperatures from OES

In general, RF low-pressure plasmas have a small degree of ionization, which makes collisional processes less efficient than in plasmas with higher electron densities; consequently, radiative processes become important. Especially, in inductively coupled low-pressure N_2-Ar plasmas, direct excitation from the ground state with radiative decay can be assumed to dominate over the production and the destruction of excited energy levels. For instance, many excited states of argon are mainly produced by electron-impact excitation from the ground state, and the quenching rate of excited argon atoms by both N_2 molecules and Ar atoms is very small compared to the radiative decay [23]. This simplification is called the corona balance and expressed in a modified Boltzmann formula as follows:

$$\ln\left(\frac{\lambda_{ij} I_{ij} \sum_{i>j} A_{ij}}{R_{ij} A_{ij} a_{1i}}\right) = -\frac{Ei}{k_B T_e} + C, \qquad (13)$$

where I_{ij}, λ_{ij}, R_{ij}, and A_{ij} are the intensity, the wavelength, the detector efficiency, and the Einstein coefficient of the spectral line for a transition from the i → the j level, respectively. The a_{1i} is the coefficient in an exponential approximation of the electron impact excitation rate coefficient from the ground state to level i, k_B is the Boltzmann constant, and E_i is the excitation energy of level i [23,24].

Figure 7(a) shows the emission spectra in the wavelength range of 670 – 860 nm from N_2-Ar plasmas at p = 1.4 mTorr and P = 500 W. Many Ar peaks, 750.4 nm, 811.5 nm, 696.5 nm ($2p_2 \rightarrow 1s_5$), 706.7 nm ($2p_3 \rightarrow 1s_5$), 738.3 nm ($2p_3 \rightarrow 1s_4$), 763.5 nm ($2p_6 \rightarrow 1s_5$), 772.4 nm ($2p_2 \rightarrow 1s_3$), 794.8 nm ($2p_4 \rightarrow 1s_3$), 810.4 nm ($2p_7 \rightarrow 1s_4$), and 801.4 nm ($2p_8 \rightarrow 1s_5$), exist. It should be noted that in low-Ar-content plasmas, these typical 2p → 1s transitions are superimposed in the transition bands of nitrogen (see the inset of Fig. 4(a)). Figure 7(b) presents a modified Boltzmann plot obtained from these Ar lines. The T_e value deduced from linear fit is indicated. For the specified operating condition, T_e is estimated to be 4.1 eV. Because this method does not incorporate a sufficient number of transitions from higher excited states, the slope of the plot has a value larger than that of the plot containing many transitions. Therefore, the deduced T_e has a value a little less than the real electron temperature. Although OES cannot result in an appropriate modified Boltzmann plot of Ar lines in low-Ar content plasmas (especially at low pressure), this method gives a reasonable estimate of T_e in medium-to-high-Ar-content plasmas. We have found that, in general, T_e decreases with growing pressure and slightly decreases with increasing argon content and power. A more elaborate OES model should take into account cascading contributions from higher excited states, collisional excitation from metastable states and photon reabsorption.

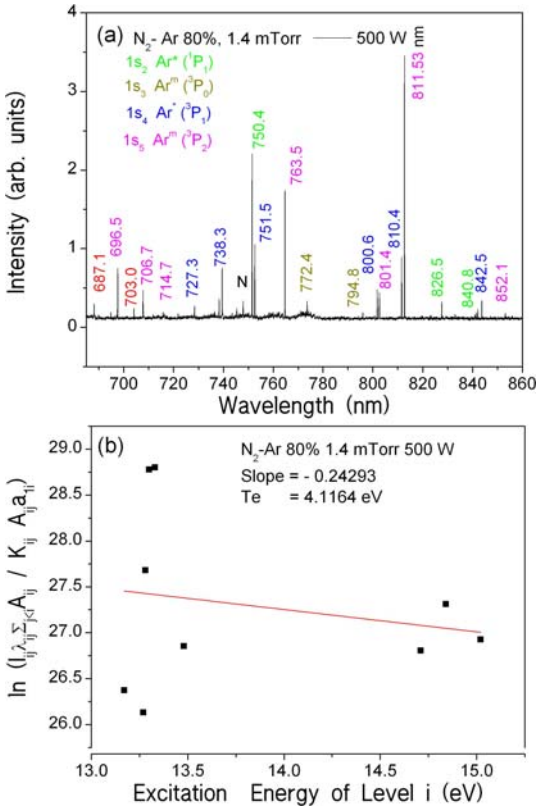

Fig. 7. (Color online) (a) Spectrum of optical emission from an inductively coupled N_2-5%Ar discharge with a range of 670 – 860 nm for the 1.4-mTorr Ar 80% plasma at 500 W. (b) The modified Boltzmann plot obtained from the Ar lines. The T_e value deduced from linear fit is indicated.

The N_2^+ first negative system band from 390 nm and 392 nm for the 391.4 nm line is fitted to obtain the N_2^+ rotational temperature. To obtain the best fit between the experimental and the synthetic spectral bands, we used a least-squares procedure [27]. A typical fitting of the measured first negative (0, 0) band spectrum with the synthetic spectrum is shown in Fig. 8(a). Good agreement between the measured spectrum and the synthetic one suggests a reasonable evaluation of T_{rot}. In Figs. 8(b) – (c), the rotational temperatures in a 95% N_2 – 5%Ar

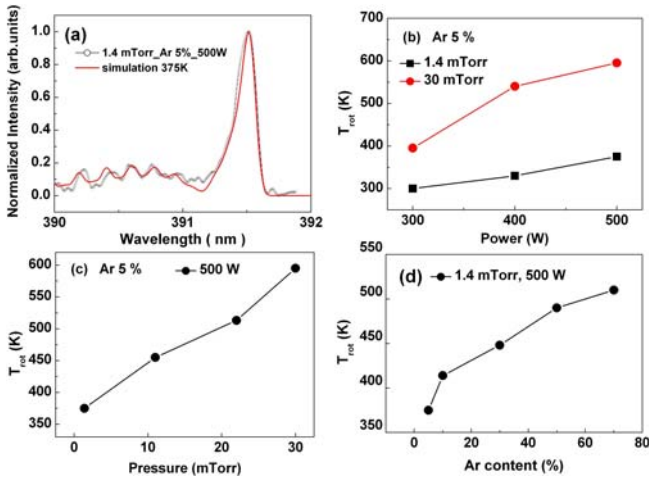

Fig. 8. (Color online) (a) A typical fitting of the measured first negative (0, 0) band spectrum with the synthetic spectrum. Rotational temperatures as functions of (b) power, (c) pressure, and (d) Ar content.

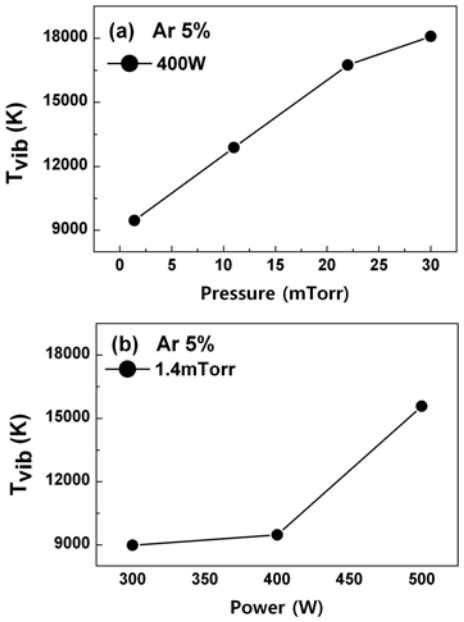

Fig. 9. Vibrational temperatures as functions of (a) pressure and (b) power.

discharge are plotted. As expected, the rotational temperature increases, as both the power and the pressure are increased due to the higher collisional loss of the electron energy. As the Ar content is increased, entrained nitrogen is converted into $N_2{}^+$ via charge transfer with Ar^+ due to the almost equal ionization potentials for argon (15.76 eV) and for molecular nitrogen (15.58 eV). The $N_2{}^+$ ion is consequently destroyed, becoming two nitrogen atoms, by dissociative recombination. As shown in Fig. 8(d), these nitrogen atoms provide energy to increase $T_{\rm rot}$ because they have a relatively high kinetic energy via exothermic dissociative recombination reactions [26].

The Boltzmann plot method was applied to the emission intensity peaks relating to $\Delta v = -1$ to estimate the vibrational temperature. The measured vibrational temperature compares well with those from previous works [26,32,33]. As shown in Figs. 9(a) – (b), the vibrational temperature increases with both increasing pressure and power. This can be accounted for from the observation that N_2 molecules in the plasma have considerable populations in the excited vibrational levels [26,38]. As the Ar content is increased, an impact of Ar^m leads to a higher population density of vibrationally-excited N_2 molecules [16]. This effect plays a more important role if the collision rate is increased by higher pressure. Also, there is a strong relationship between the vibrational distribution function of molecules and the electron density.

IV. CONCLUSION

The properties of inductively coupled N_2-Ar plasmas have been studied to understand the effect of various operating parameters. The electron temperature, the rotational and the vibrational temperatures, and the ratios of the emission intensities from plasma species were measured by using optical emission spectroscopy. Along with these, a Langmuir probe measurement was also performed. The plasma density was found to increase with increasing power and Ar content. The electron temperature decreased slightly with increasing Ar content. The intensity ratios of representative peaks in the N_2-Ar plasmas were measured, and this allowed us to estimate the evolutions of the number densities of neutral species with determined rate coefficients. Although some differences between the single and double probe results and OES exist, those differences are in a tolerable range. The EEPFs of low-pressure inductively coupled N_2-Ar plasmas are found to be Maxwellian in both the E-mode and the H-mode. The modified Boltzmann plots give values comparable to T_e measured by using a single probe and provide a reasonable estimate of T_e. The gas temperature shows an increase as both the power and the pressure are increased. At a pressure of 1.4 mTorr, the gas temperature increases with increasing Ar content. The vibrational temperature of N_2 increases with increasing pressure and power. Both the rotational and the vibrational temperatures increase with increasing Ar content, thus making nitrogen plasmas more reactive. The comparability of the energy levels of the excited states in N_2, N, and Ar induces rich plasma chemical reactions, and Ar^m plays an important role. Although some uncertainty is associated with the rate coefficients used, the simple model presented in this work can provide a useful tool for characterizing inductively coupled N_2-Ar plasmas.

ACKNOWLEDGMENTS

This work was supported by Dong-A University.

REFERENCES

[1] N. Itagaki, S. Iwata, K. Muta, A. Yonesu, S. Kawakami, N. Ishii and Y. Kawai, Thin Solid Films **435**, 259 (2003).
[2] R. W. McCullough, J. Geddes, J. A. Croucher, J. M. Woolsey, D. P. Higgins, M. Schlapp and H. B. Gilbody, J. Vac. Sci. Technol., A **14**, 152 (1996).
[3] H. Nagai, S. Takashima, M. Hiramatsu, M. Ori and T. Goto, J. Appl. Phys. **91**, 2615 (2002).
[4] T. Czerwiec, F. Greer and D. B. Graves, J. Phys. D: Appl. Phys. **38**, 4278 (2005).
[5] T. Nakano, S. Kumagai and S. Samukawa, J. Appl. Phys. **92**, 2290 (2002).
[6] S. Tada, S. Takashima, M. Ito, M. Hori, T. Goto and Y. Sakamoto, J. Appl. Phys. **88**, 1756 (2000).
[7] D. Voulot, R. W. McCullough, W. R. Thompson, D. Burns, J. Geddes, Q. J. Gosimini, E. Nelson, P. P. Chow and J. Klaassen, J. Vac. Sci. Technol., A **16**, 3434 (1998).
[8] M. A. Worsley, S. F. Bent, N. C. M. Fuller and T. Dalton, J. Appl. Phys. **100**, 083301 (2006).
[9] E. G. Thorsteinsson and J. T. Gudmundsson, Plasma Sources Sci. Technol. **18**, 045001 (2009).
[10] T. Kitajima, T. Nakano, S. Samukawa and T. Makabe, Plasma Sources Sci. Technol. **17**, 024018 (2008).
[11] J. Henriques, E. Tatarova, F. M. Dias and C. M. Ferreira, J. Appl. Phys. **91**, 5632 (2002).
[12] E. Abdel-Fattah, M. Bazavan and H. Sugai, J. Appl. Phys. **110**, 113303 (2011).
[13] N. Kang, N. Britun, S. Oh, F. Gaboriau and A. Ricard, J. Phys. D: Appl. Phys. **42**, 12001 (2009).
[14] T. Kimura and H. Kasugai, J. Appl. Phys. **108**, 033305 (2010).
[15] X-J. Huang, Y. Xin, L. Yang, Q-H. Yuan and Z-Y. Ning, Phys. Plasmas **15**, 113504 (2008).
[16] M. A. Song, Y. W. Lee and T. H. Chung, Phys. Plasmas **18**, 023504 (2011).
[17] T. H. Chung, Y. W. Lee, H. M. Joh and M. A. Song, AIP Advances **1**, 032136 (2011).
[18] J. L. Jauberteau and I. Jauberteau, Plasma Sources Sci. Technol. **17**, 015019 (2008).
[19] N. Bibinov, H. Halfmann and P. Awakowicz, Plasma Sources Sci. Technol. **17**, 035004 (2008).
[20] B. Clarenbach, B. Lorenz, M. Cramer and N. Sadeghi, Plasma Sources Sci. Technol. **12**, 345 (2003).
[21] C. C. Lin, Contrib. Plasma Phys. **44**, 405 (2004).
[22] G. A. Piech, J. B. Boffard, M. F. Gehrke, L. W. Anderson and C. C. Lin, Phys. Rev. Lett. **81**, 309 (1998).
[23] F. J. Gordillo-Vazquez, M. Camero and C. Gomez-Aleixandre, Plasma Sources Sci. Technol. **15**, 42 (2006).
[24] C. Foissac, C. Dupret and P. Supiot, J. Phys. D: Appl. Phys. **42**, 015206 (2009).
[25] M. Tuszewski, J. Appl. Phys. **100**, 053301 (2006).
[26] E. J. Tonnis and D. B. Graves, J. Vac. Sci. Technol., A **20**, 1787 (2002).
[27] S. Y. Moon and W. Choe, Spectrochim. Acta, Part B **58**, 249 (2003).
[28] T. Sakamoto, H. Matsuura and H. Akatsuka, J. Appl. Phys. **101**, 023307 (2007).
[29] J. C. Thomaz, J. Amorim and C. F. Souza, J. Phys. D: Appl. Phys. **32**, 3208 (1999).
[30] L. M. Isola, B. J. Gomez and V. Guerra, J. Phys. D: Appl. Phys. **43**, 015202 (2010).
[31] J-H. Ku, Y-K. Lee and C-W. Chung, Phys. Plasmas **17**, 043508 (2010).
[32] N. Britun, M. Gaillard, A. Ricard, Y. M. Kim and J. G. Han, J. Phys. D: Appl. Phys. **40**, 1022 (2007).
[33] V. Linss, H. Kupfer, S. Peter and F. Richter, J. Phys. D: Appl. Phys. **37**, 1935 (2004).
[34] W-Y. Ding, J. Xu, W-Q. Lu, X-L. Deng and C. Dong, Phys. Plasmas **16**, 053502 (2009).
[35] R. M. Frost, P. Awakowicz, H. P. Summers and N. R. Badnell, J. Appl. Phys. **84**, 2989 (1998).
[36] J. B. Boffard, G. A. Piech, M. F. Gehrke, L. W. Anderson and C. C. Lin, Phys. Rev. A **59**, 2749 (1999).
[37] A. Dasgupta, M. Blaha and J. L. Giuliani, Phys. Rev. A **61**, 012703 (1999).
[38] P. A. Sa and J. Loureiro, J. Phys. D: Appl. Phys. **30**, 2320 (1997).